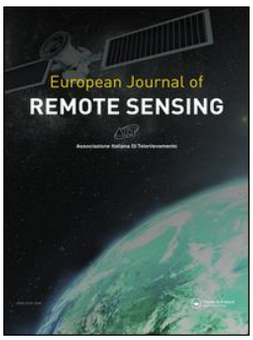

European Journal of Remote Sensing

ISSN: (Print) 2279-7254 (Online) Journal homepage: http://www.tandfonline.com/loi/tejr20

Data analysis tools for persistent scatterer interferometry based on Sentinel-1 data

Núria Devanthéry, Michele Crosetto, Oriol Monserrat, Bruno Crippa & Marek Mróz

To cite this article: Núria Devanthéry, Michele Crosetto, Oriol Monserrat, Bruno Crippa & Marek Mróz (2018): Data analysis tools for persistent scatterer interferometry based on Sentinel-1 data, European Journal of Remote Sensing, DOI: 10.1080/22797254.2018.1554981

To link to this article: https://doi.org/10.1080/22797254.2018.1554981

Published online: 14 Dec 2018.

EUROPEAN JOURNAL OF REMOTE SENSING
https://doi.org/10.1080/22797254.2018.1554981

Taylor & Francis
Taylor & Francis Group

Data analysis tools for persistent scatterer interferometry based on Sentinel-1 data

Núria Devanthéry[a], Michele Crosetto[a], Oriol Monserrat[a], Bruno Crippa[b] and Marek Mróz[c]

[a]Division of Geomatics, Centre Tecnològic de Telecomunicacions de Catalunya (CTTC), Castelldefels (Barcelona), Spain; [b]Department of Earth Sciences, University of Milan, Milan, Italy; [c]Institute of Geodesy, University of Warmia and Mazury in Olsztyn, Olsztyn, Poland

ABSTRACT

This paper describes a Persistent Scatterer Interferometry procedure to process Sentinel-1 SAR data. Its most original part includes a set of tools to perform two key processing stages: a first 2 + 1D phase unwrapping, prior to atmospheric filtering, and a second 2 + 1D phase unwrapping, to generate the deformation time series. These tools address two fundamental aspects of a Persistent Scatterer Interferometry processing chain: the quality control of the intermediate and final results, and the generation of quality indices to characterise such results. The effectiveness of the proposed tools is illustrated using a case study located in Catalonia (Northern Iberian Peninsula).

ARTICLE HISTORY
Received 30 October 2017
Revised 27 November 2018
Accepted 29 November 2018

KEYWORDS
SAR; interferometry; data analysis; deformation monitoring

Introduction

Persistent Scatterer Interferometry (PSI) is a powerful radar-based remote sensing technique able to measure and monitor displacements of the Earth's surface. For a general PSI review see Crosetto, Monserrat, Cuevas-González, Devanthéry, and Crippa (2016). This paper describes a procedure to process and analyse PSI data coming from the C-band sensors on board the satellites of the Sentinel-1 (S-1) mission. This mission is the first of the five missions that ESA is developing for the Europe's Copernicus Programme. It includes two polar-orbiting satellites (Sentinel-1A and Sentinel-1B) performing C-band Synthetic Aperture Radar (SAR) imaging. The two satellites have been launched on 3 April 2014 and 25 April 2016, respectively.

Compared to previous C-band missions, the two S-1 sensors have enhanced data acquisition throughput (Torres et al., 2012), which results in an increased deformation monitoring potential. By using the Interferometric Wide Swath (IWS) mode, which is the standard S-1 acquisition mode over land, the S-1 sensors acquire data with a swath of 250 km using the TOPS (Terrain Observation by Progressive Scan) imaging mode. A key characteristic is given by the revisiting time: S-1A alone has a 12-day revisiting cycle, while the cycle becomes 6-days using the twin satellites S-1A and S-1B. This represents a remarkable improvement with respect to the revisiting time capability of previous missions, like ERS and Envisat. This results in a reduced temporal decorrelation of the SAR data. An additional important characteristic of the S-1 data is the reduced orbital tube with respect to previous SAR missions: in case of S-1 this tube has an approximate diameter of 100 m, while for ERS and Envisat the tube was of several hundreds of meters (Geudtner, Torres, Snoeij, Davidson, & Rommen, 2014). This results in a reduced geometric decorrelation of the S-1 data (Gatelli et al., 1994). The reduced temporal and geometric decorrelation caused an enhanced coherence of the interferometric S-1 data. A final important characteristic of the S-1 is that it benefits from the free, full and open data policy adopted by the Copernicus Programme. This is a key element to foster data exploitation by academic and commercial initiatives.

The potential of S-1 based PSI has been documented in the literature. Barra et al. (2016) and Barra et al. (2017) use S-1 data for landslide detection and mapping. A mega-landslide study is described in Dai et al. (2016), while a tunnelling-induced landslide is described in Bayer, Simoni, Schmidt, and Bertello (2017). Different studies concern volcano monitoring, for example see González et al. (2015) and De Luca et al. (2016). Examples related to subsidence monitoring are discussed in Crosetto, Devanthéry, Cuevas-González, Monserrat, and Crippa (2015) and Shirzaei, Bürgmann, and Fielding (2017). The monitoring of mining-induced deformation is described in Ng, Ge, Du, Wang, and Ma (2017), while a case of infrastructure monitoring (long bridges) is described in Huang, Crosetto, Monserrat, and Crippa (2017). Novellino et al. (2017) assess the feasibility of a nation-wide S-1 ground deformation mapping.

CONTACT Michele Crosetto mcrosetto@cttc.cat Centre Tecnològic de Telecomunicacions de Catalunya (CTTC), Av. Gauss, 7, Barcelona, Castelldefels E-08860, Spain

The S-1 wide area coverage associated with its short revisiting cycle result in the availability of big volumes of data. This requires appropriate tools to process and analyse these PSI data. In this paper we propose a set of data processing and analysis tools that are related to a key PSI processing step: phase unwrapping. In particular, it refers to the so-called 2 + 1D phase unwrapping described in Devanthéry, Crosetto, Monserrat, Cuevas-González, and Crippa (2014). The proposed tools address two key aspects:

- The quality control of some data processing and analysis procedures. This is an important aspect while processing very large datasets: automatic or, at least, semi-automatic procedures are especially useful.
- The automatic generation of quality indices to characterise: (i) the intermediate PSI results; the quality indices can be used in the subsequent processing steps; (ii) the final PSI results; in this case the quality indices represent a key input for the exploitation and interpretation of the results.

The paper is organised as follows. Section 2 provides an overview of the entire data processing and analysis procedure implemented by the authors. Section 3 discusses in detail the proposed data analysis tools related to the 2 + 1D phase unwrapping. Section 4 describes the results obtained with a dataset that covers Catalonia (Spain). This illustrates the proposed data analysis tools and the deformation PSI results obtained over the study area. Section 5 contains the conclusions of this work.

Overview of the entire procedure

The procedure used in this study is based on the PSIG approach proposed in Devanthéry et al. (2014). The PSIG chain, PSI chain of the Geomatics Division of CTTC, which was mainly focused on extending the PSI processing to wide areas, has been successfully applied using X-band data (Devanthéry et al., 2014). In this study, the chain is used with S-1 data collected in the IWS mode, that is data with a 250-km swath acquired using the TOPS imaging mode. Three sub-swaths are acquired by steering the beam in range, while, by electronically steered the beam from backward to forward in the azimuth direction, several bursts are acquired. Therefore, each of the three sub-swath images consists of a series of bursts (sub-images). The bursts are synchronised from pass to ensure the alignment of interferometric pairs. An IWS SLC product contains one image per sub-swath and one per polarisation channel, for a total of three images for single polarisation, or six images for dual polarisation.

We describe in the following the PSI procedure to process S-1 interferometric data. The procedure requires a large set of N SAR images and a redundant network of M interferograms, where $M \gg N$. The full procedure consists in the following steps:

- Pre-processing. Due to the TOPS characteristics, the S-1 data need extra processing with respect to the standard StripMap processing (Yague-Martinez et al., 2016). This mainly affects the image co-registration step which, due to the high Doppler rate caused by the azimuth antenna beam steering, needs to be very accurate ($1/10^3$ pixels in azimuth, see Prats-Iraola, Scheiber, Marotti, Wollstadt, & Reigber, 2012). To achieve such an accuracy, a two-step process has been proposed by different authors (Prats-Iraola et al., 2012; Scheiber & Moreira, 2000; Yague-Martinez et al., 2016): (i) a pixel-level co-registration is carried out by using classical SAR image co-registration methods. This can be done using orbit information or cross-correlation methods; then (ii) an accuracy refinement is obtained by using the Spectral Diversity (Prats-Iraola et al., 2012; Scheiber & Moreira, 2000). The pre-processing is performed burst-wise; it is then followed by a merging to form sub-swaths of interferograms and amplitude images.
- Selection of the set of Persistent Scatterer (PS) candidates. We used the Dispersion of Amplitude (DA) criterion, instead of the so-called Cousin PSs (CPS), that is PSs characterised by a moderate spatial phase variation to ensure a correct phase unwrapping, which are described in Devanthéry et al. (2014). One of the reasons to use the DA instead of CPS is because the small S-1 orbital tube causes smaller Residual Topographic Errors (RTE) and hence a less error-prone phase unwrapping.
- First stage of the so-called 2 + 1D phase unwrapping. Firstly, a spatial 2D phase unwrapping using the Minimum Cost Flow method (Costantini, 1998; Costantini, Farina, & Zirilli, 1999) is performed over multi-looked interferograms. This is followed by a 1D phase unwrapping performed pixel wise over the M interferograms, which uses a robust iterative least squares procedure (Baarda, 1968; Björck, 1996; Förstner, 1986). This procedure works on the so-called residuals of the interferometric observation equations (with one residual per each of the M interferograms), and fully exploits the integer nature of the unwrapping errors, see for details Devanthéry et al. (2014). It is worth to note that this stage generates a set of N unwrapped phase images, which are temporally ordered in correspondence of the dates of the processed SAR images. The specific data analysis

tools related to this 2 + 1D phase unwrapping are described in the following section.

- Atmospheric filtering. Using the unwrapped phases images coming from the previous step, an estimation of the Atmospheric Phase Screen (APS) is performed using a set of spatio-temporal filters (Berardino, Fornaro, Lanari, & Sansosti, 2002; Ferretti, Prati, & Rocca, 2001). The APSs are then removed from the original interferograms. This operation is typically performed at full resolution, to carry out the subsequent processing step using single look data. However, it can also be performed on multi-look data.
- Deformation velocity and RTE estimation. Using the method of the periodogram and a linear deformation model, the deformation velocity and the RTE are estimated from the wrapped APS-free interferograms. An extension of the two-parameter model can be optionally used to account for the thermal expansion (Monserrat, Crosetto, Cuevas, & Crippa, 2011). The RTE phase component is then removed from the wrapped APS-free interferograms. Note that the same operation can be carried out for the deformation velocity, which then, in a later stage, is added back to the deformation time series. The same procedure can be done with the thermal expansion component.
- Second stage of the 2 + 1D phase unwrapping. This step, which is performed on M APS- and RTE-free interferograms, is used to generate the final deformation time series. This stage generates, for each processed pixel, a set of N deformation estimates, which are temporally ordered in correspondence of the acquisition dates of the processed SAR images. It is important to underline that the time series generation does not make any deformation model assumption. The deformation velocity map is derived starting from the time series. The data analysis tools related to this stage are described in the following section.
- The final step is the geocoding of the PSI results.

Analysis tools related to 2 + 1D phase unwrapping

This section discusses the data analysis tools related to the 2 + 1D phase unwrapping. The phase unwrapping is performed twice in the PSI procedure: (i) prior to atmospheric filtering and (ii) during deformation time series generation. In the following, we treat separately these two stages. The first stage, which is prior to the atmospheric filtering, includes the analyses detailed in the following.

1) Analysis of the 2 + 1D phase unwrapping residuals. This is a data quality control step. The analysis is carried out using the plot that displays the residuals (one residual for each interferogram) of each processed PS. Under optimal conditions, such residuals go to zero at the last iteration of the 2 + 1D phase unwrapping, indicating that all the phase unwrapping errors are properly detected and corrected. However, this may not occur in at least two cases: the presence of anomalous interferograms or images in the processed dataset. Therefore, this analysis is focused on two issues:
   - Identify anomalous interferograms. They correspond to large residual values in correspondence to (at least) one interferogram. They can be due to problems related to the interferogram generation. The typical action in this case is to identify the anomalous interferogram, correct or remove it from the dataset.
   - Identify anomalous images. An anomalous image, which can be typically due to errors in the image extraction or image co-registration, affects all the interferograms that contain it. It is therefore identified by large residual values in correspondence to a set of interferograms that shares the same image. The action is identifying the anomalous image, correct or remove it from the dataset.
2) Control of the 2 + 1D phase unwrapping outcomes. This is a data quality control step. Its objective is to check the quality of the phase unwrapping values coming from the first 2 + 1D phase unwrapping stage. Three classes are defined, “Good”, “Fair” and “Warning” (Devanthéry et al., 2014): if the ratio (Cor_%) between the number of corrections and the number interferograms connected with an image is less than 30% for all the images of a given pixel, then the pixel is labelled as “Good”. It is “Fair” if Cor_% is between 30% and 40%, and “Warning” if Cor_% is above 40%. A typical action is to discard in the subsequent processing steps all the pixel labelled “Warning”. An alternative and more complex action is to run a second iteration of the 2 + 1D phase unwrapping. For instance, this is needed if a key area of interest is insufficiently covered by “Fair” and “Good” pixels.
3) Generation of a 2 + 1D phase unwrapping quality index. The objective of this step is to automatically generate a quality index to characterise this intermediate PSI result. This index, which is defined pixel wise, is given by the standard deviation of all residuals of a given pixel. Assuming that there are no phase unwrapping errors (they are controlled in the previous analysis step), this index reflects

the closure errors ($\phi_{ij}+\phi_{jk}+\phi_{ki}\neq 0$, where ϕ is the interferometric phase, and i, j and k are three images) that characterise the multi-look data: the smaller is the closure error, the higher is the quality of the pixel at hand. It is worth noting that this index does not work with single-look data that have no closure errors. This information on the quality of single pixels characterises an intermediate product of the PSI chain (the stack of unwrapped image phases) and can be used in the subsequent processing step: the atmospheric filtering, where the importance of every single pixel can be weighted according to the above index.

The second stage, which is used to generate the deformation time series, includes the analyses detailed below.

1) Analysis of the 2 + 1D phase unwrapping residuals. Like in the first stage, this data quality control step can be used to detect the presence of anomalous interferograms or images, and to correct or remove them.
2) Generation of a quality index for each image of a given deformation time series. The deformation time series contain an estimated deformation in correspondence of the date of each processed SAR image. The quality index associated to each image of a time series is given by the number of corrections. This provides a complete information that can be used to assess the quality of the time series. This represents a key metadata of the time series, which can be used in the interpretation and exploitation of the PSI results.
3) Generation of a quality index for the deformation time series (pixel wise). This is the same index used in the first stage of the analysis (to characterise an intermediate PSI result). It can be only generated using multi-look data. In this case it concerns the quality of a final product (the deformation time series): it represents a useful metadata for the interpretation of the PSI results.

Discussion of the results

The results of this study concern a large part of Catalonia (Northern Iberian Peninsula), see Figure 1. The covered area is approximately 31,000 km^2. A total of 64 S-1A images were used, see Table 1, covering the period from March 2015 to May 2017. The data processing was performed sub-swath wise. Some of the images were discarded during the first steps of the processing: the final dataset used in this study includes 60 images in sub-swath 1, 56 images in sub-swath 2 and 59 images in sub-swath 3.

We firstly consider the analysis of the first stage (2 + 1D phase unwrapping prior to atmospheric filtering), which was performed on 10 by 2 multi-looked data. This analysis was performed sub-swath

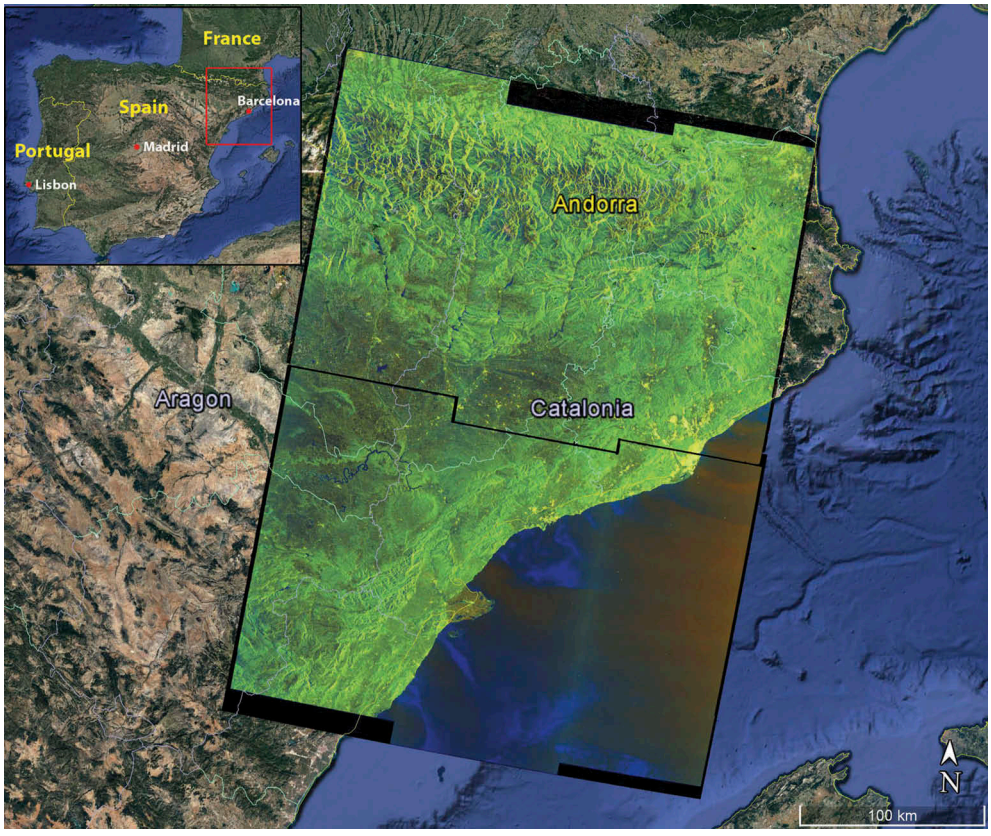

Figure 1. Footprint of the processed image and area of interest (red square). The area is covered by 3 sub-swaths and 30 bursts.

Table 1. Acquisition date and orbit of the 64 images used in this work.

Date	Orbit	Date	Orbit	Date	Orbit
06/03/2015	4907	31/12/2015	9282	02/10/2016	13307
18/03/2015	5082	12/01/2016	9457	14/10/2016	13482
30/03/2015	5257	24/01/2016	9632	26/10/2016	13657
11/04/2015	5432	05/02/2016	9807	07/11/2016	13832
23/04/2015	5607	17/02/2016	9982	19/11/2016	14007
05/05/2015	5782	29/02/2016	10157	01/12/2016	14182
17/05/2015	5957	12/03/2016	10332	13/12/2016	14357
29/05/2015	6132	24/03/2016	10507	25/12/2016	14532
04/07/2015	6657	05/04/2016	10682	06/01/2017	14707
16/07/2015	6832	17/04/2016	10857	18/01/2017	14882
28/07/2015	7007	29/04/2016	11032	30/01/2017	15057
09/08/2015	7182	11/05/2016	11207	11/02/2017	15232
21/08/2015	7357	04/06/2016	11557	23/02/2017	15407
02/09/2015	7532	28/06/2016	11907	07/03/2017	15582
14/09/2015	7707	10/07/2016	12082	19/03/2017	15757
26/09/2015	7882	22/07/2016	12257	31/03/2017	15932
08/10/2015	8057	03/08/2016	12432	12/04/2017	16107
01/11/2015	8407	15/08/2016	12607	24/04/2017	16282
13/11/2015	8582	27/08/2016	12782	06/05/2017	16457
25/11/2015	8757	08/09/2016	12957	18/05/2017	16632
07/12/2015	8932	20/09/2016	13132	30/05/2017	16807
19/12/2015	9107				

wise. Figure 2 illustrates the 2 + 1D phase unwrapping residuals at the first and last iteration for three different datasets of sub-swath 1. In the first dataset (upper), which consists of 60 images and 735 interferograms, the 2 + 1D phase unwrapping was successful for all pixels: all residuals at the last iteration are close to zero. The second dataset (middle) contains 60 images and 741 interferograms. In the residuals of the last iteration there are 6 clusters of residuals different from zero, which correspond to 6 interferograms. All these six interferograms showed to have problems, probably originated during the pre-processing (interferogram generation). It is worth noting that the pre-processing is done burst-wise. This dataset involves eight burst for each interferogram, that is a total of 5928 bursts. With such a large dataset it is useful to have a procedure to detect automatically the anomalous interferograms. The third dataset consists of 62 images and 807 interferograms. In the last iteration there are 16 clusters of big residuals, which correspond to 16 interferograms. In this case all these interferograms correspond to the same image, which was affected by co-registration errors. The image was removed from the dataset. Also this example shows the effectiveness of the data quality procedure.

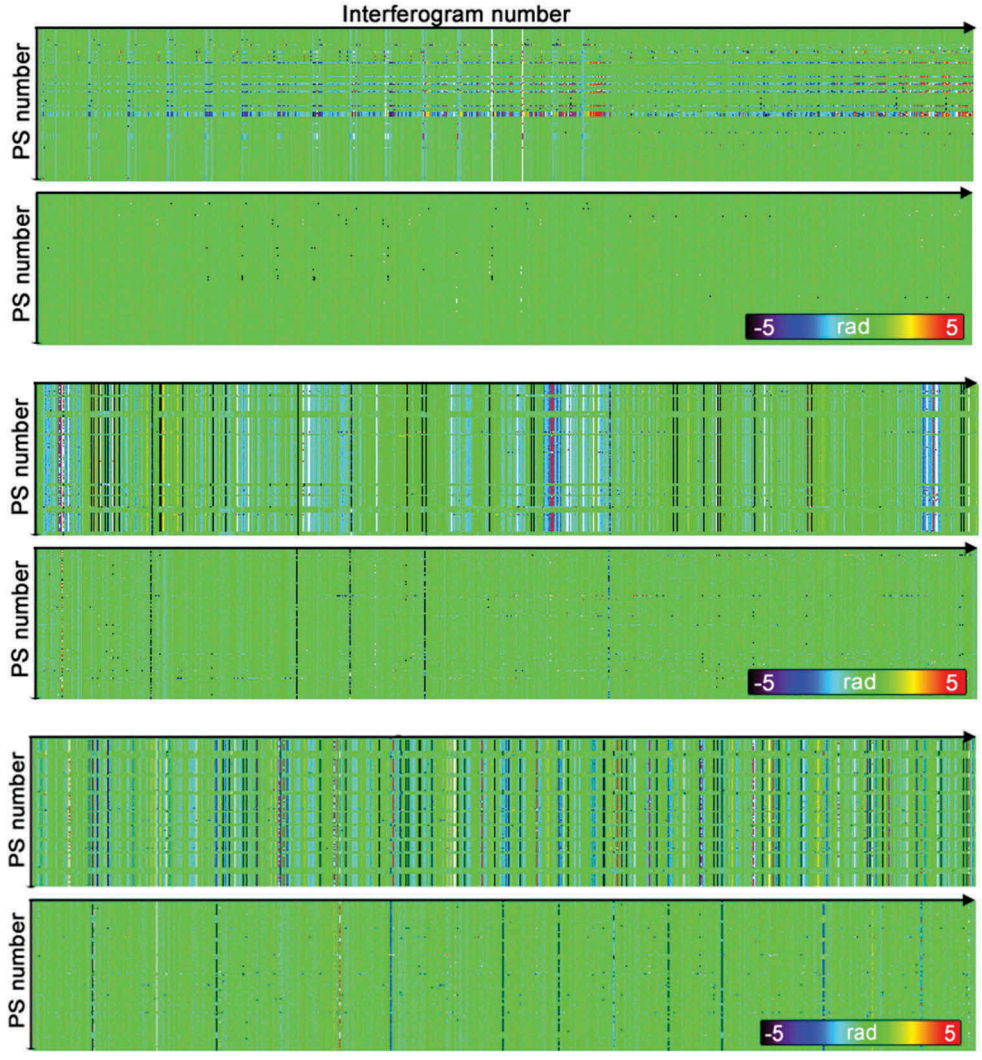

Figure 2. 2 + 1D phase unwrapping residuals at the first (above) and last iteration (below) for three different datasets.

Once the anomalous interferograms and images were properly corrected or removed, the results of the final 2 + 1D phase unwrapping prior atmospheric filtering were generated sub-swath wise. For sub-swath 1 we used 60 images and 735 interferograms (temporal baseline below 200 days); for sub-swath 2 we used 56 images and 372 interferograms (temporal baseline below 108 days); and for sub-swath 3 we used 59 images and 370 interferograms (temporal baseline below 100 days). The smaller baselines of sub-swath 2 and 3, which mainly cover rural areas, take into account the fast temporal decorrelation in such areas. The quality control of these results was based on the three-class map showed in Figure 3. In this map, green corresponds to "Good", yellow to "Fair" and red to "Warning" points. The number of pixels per each class is shown in Table 2: 11,9% of the pixels are labelled as "Warning". They are mainly clustered in the upper and right part of Figure 3.

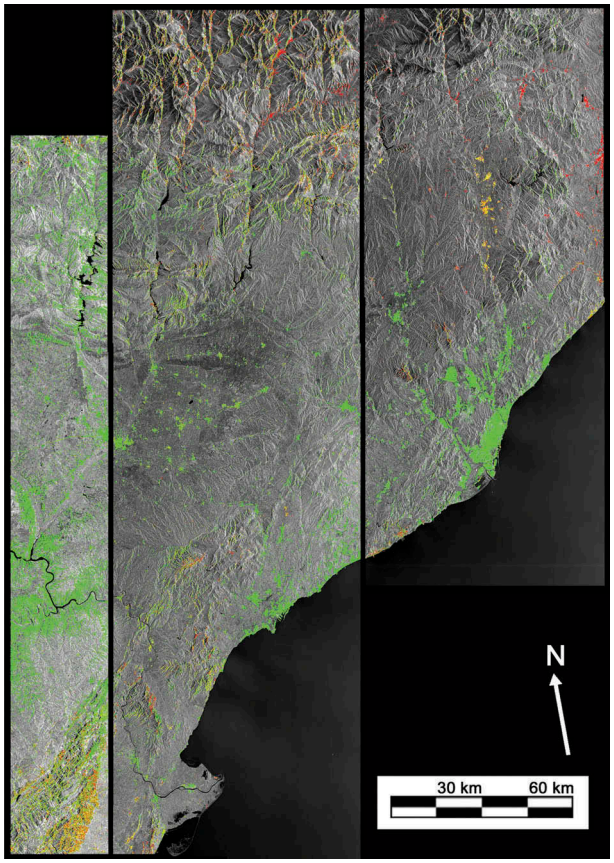

Figure 3. Three-class maps of the results of 2 + 1D phase unwrapping prior to atmospheric filtering: "Good" (green), "Fair" (yellow) and "Warning" (red).

Table 2. Number of pixels classified as "Good", "Fair" and "Warning" for each processed sub-swath.

	Swath 1	Swath 2	Swath 3	Percentage (%)
Good	50039	110621	129009	68.91
Fair	5506	46660	28436	19.18
Warning	6424	30978	12674	11.91
Total	61969	188259	170119	

These pixels were removed in the subsequent processing steps.

Once the "Warning" pixels were removed, we generated the 2 + 1D phase unwrapping quality index by computing the standard deviation of the residuals for each processed pixel. Figure 4 shows, for two sub-images of the dataset (the town of Montmeló and the port of Barcelona), the quality index map and the associated estimated deformation velocity. In the case of Montmeló (Figure 4, left), most of the quality index values are close to zero, including those located in the deformation area. In the port of Barcelona (Figure 4, right), there are some clusters of pixels with high standard deviation of the residuals, which mostly coincide with non-zero deformation velocity values: these pixels were underweighted in the subsequent atmospheric filtering stage.

The removal of the atmospheric component of each image was applied on single-look 1 by 1 interferogram. Then a second iteration of the 2 + 1D phase unwrapping (time series generation) was performed. The main outcomes of this stage are the deformation velocity map and the deformation time series. Figure 5 shows the deformation velocity map in radar geometry, which refers to the Line of Sight, superposed to a mean SAR amplitude image. This map includes more than 933,000 measured PSs over an area of around 22,500 km^2, with a density of about 41 PS/km^2. These PSs correspond to the "Good" and "Fair" pixels from Figure 3. The standard deviation of the velocity in urban areas is 0.94 mm/yr and in non-urban areas is 1.14 mm/yr. However, in some mountain and countryside areas the measurements seem to be noisy (see the blue colours in the upper and left part of Figure 5). Some of them correspond to "Fair" pixels, see Figure 3. The deformation map contains some interesting deformation areas related to mining activities, water extraction, terrain compaction, etc.

Figure 6 shows the geocoded deformation velocity superposed to an optical image from Google Earth, which concerns the town of Montmeló. This area includes a maximum subsidence of 14 mm/yr and an uplift of about 5 mm/yr. Figure 7 shows three examples of time series with the associated quality index per each image. The first time series (upper left) shows an uplift up to 17 mm, the second one (upper right) displays a subsidence up to 35 mm, while the third one (below) shows a stable point, with a standard deviation 1.02 mm. All images of the three time series are classified as "Good": the number of corrections is mostly zero.

Figure 8 shows the geocoded deformation velocity over the mining area of Sallent and Balsareny, where land subsidence up to 20 mm/yr was measured. Figure 9 shows three examples of time series with the associated quality index. The first time series (upper left) shows a subsidence, which accumulates

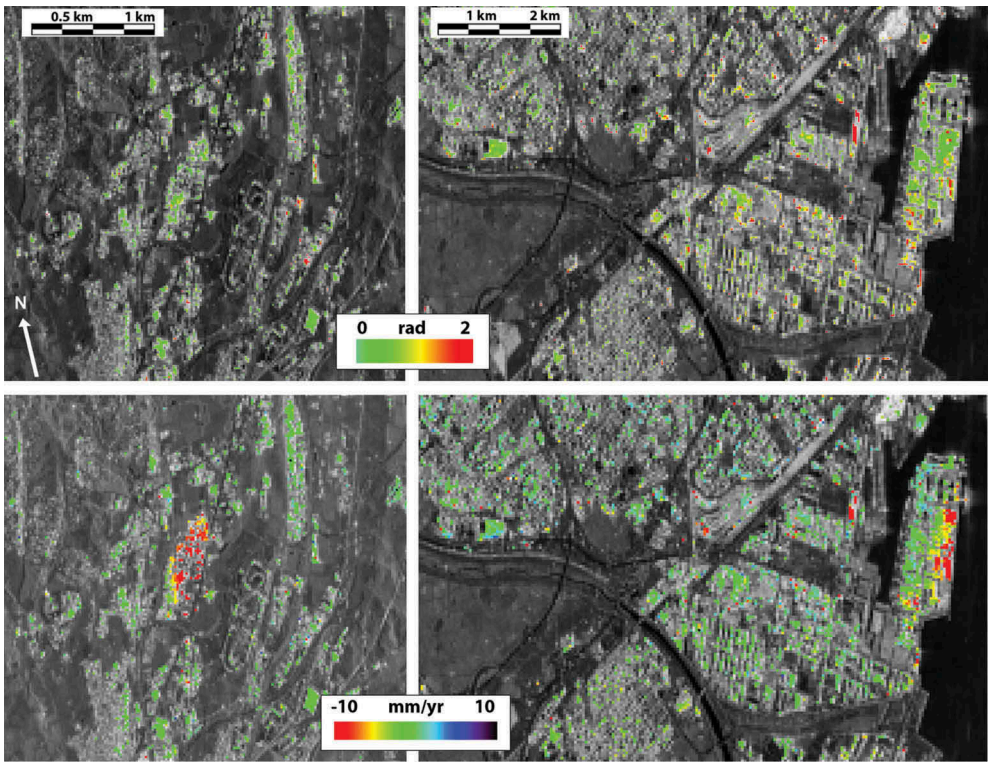

Figure 4. Map of the 2 + 1D phase unwrapping quality index (above) and deformation velocity map (below), computed over the town of Montmeló (left) and the port of Barcelona (right). The maps are superposed to the mean amplitude image.

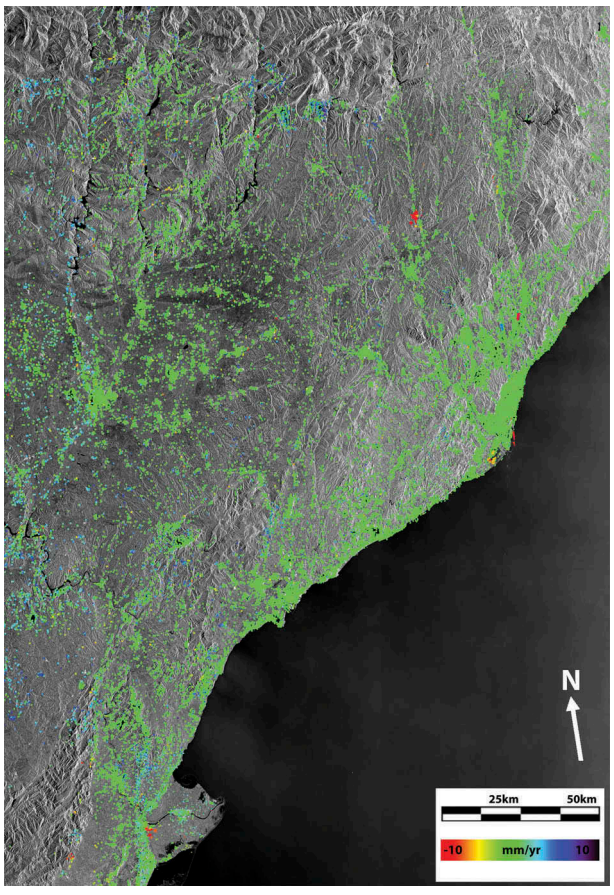

Figure 5. Deformation velocity map in radar geometry, superposed to a mean SAR amplitude image.

40 mm in 26 months. This point is classified as "Good" because the number of corrections is below 3 for all images. The second time series (upper right) corresponds to a "Fair" point. The first part of the time series, between 17/05/2015 and 29/05/2015, shows phase unwrapping related problems: in this part are concentrated up to 7 corrections per image. Note that "Fair" point indicates that the point has to be analysed before accepting it. In this case, the index points out an error in the time series. An example of "Warning" time series, which accumulates a deformation of 60 mm in 26 months, is shown in the bottom part of Figure 9. The image 05/04/2016 has 12 corrections, indicating that the 2 + 1D phase unwrapping is not reliable. The deformation in correspondence of this image has a relatively small spike of approximately 15 mm, which however affects only this image.

Conclusions

In this paper, a procedure to process and analyse S-1 PSI data have been described. The procedure represents an evolution of the PSIG approach proposed in Devanthéry et al. (2014). It includes a set of tools to perform two key processing stages: the 2 + 1D phase unwrapping prior to atmospheric filtering, and the 2 + 1D phase unwrapping to generate the deformation time series. The proposed tools address two fundamental aspects of any advanced PSI processing chain: the quality control of the results of the main processing stages, and the generation of quality indices to characterise the intermediate and the final

Figure 6. Color-coded and geocoded deformation velocity over an area surrounding the town of Montmeló (Barcelona). The background image is an optical image from Google Earth. White circles show the position of the deformation time series of Figure 7.

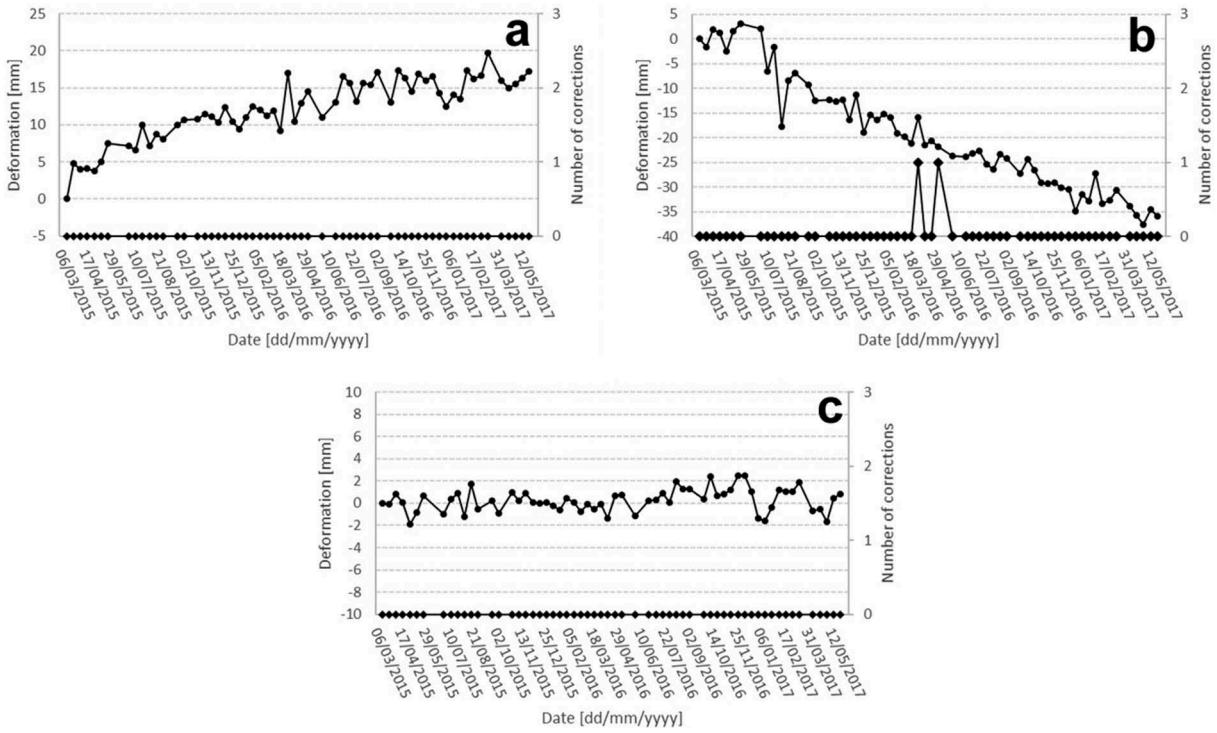

Figure 7. Three examples of time series of points located in the area shown in Figure 6 (see white circles). Each image of the time series (circles in the upper line) has associated a quality index (diamonds in the lower line).

results of the PSI chain. In particular, the following tools have been proposed:

- The analysis of the 2 + 1D phase unwrapping residuals, which works prior to atmospheric filtering and during time series generation. This is a data quality control step, which can be used to identify, correct or remove anomalous interferograms or images. As it has been shown in the experimental part, where anomalous interferograms (due to interferogram generation errors) and anomalous images (due to image co-registration errors) have been identified, this tool is particularly useful to process very large datasets.
- The control of the 2 + 1D phase unwrapping outcomes, which is based on three classes: "Good", "Fair" and "Warning". This data control step is used to discard doubtful ("Warning") unwrapped phase data in the subsequent processing steps. An example of three-class map has been illustrated in this paper.
- The generation of a 2 + 1D phase unwrapping quality index. This index, which characterises an

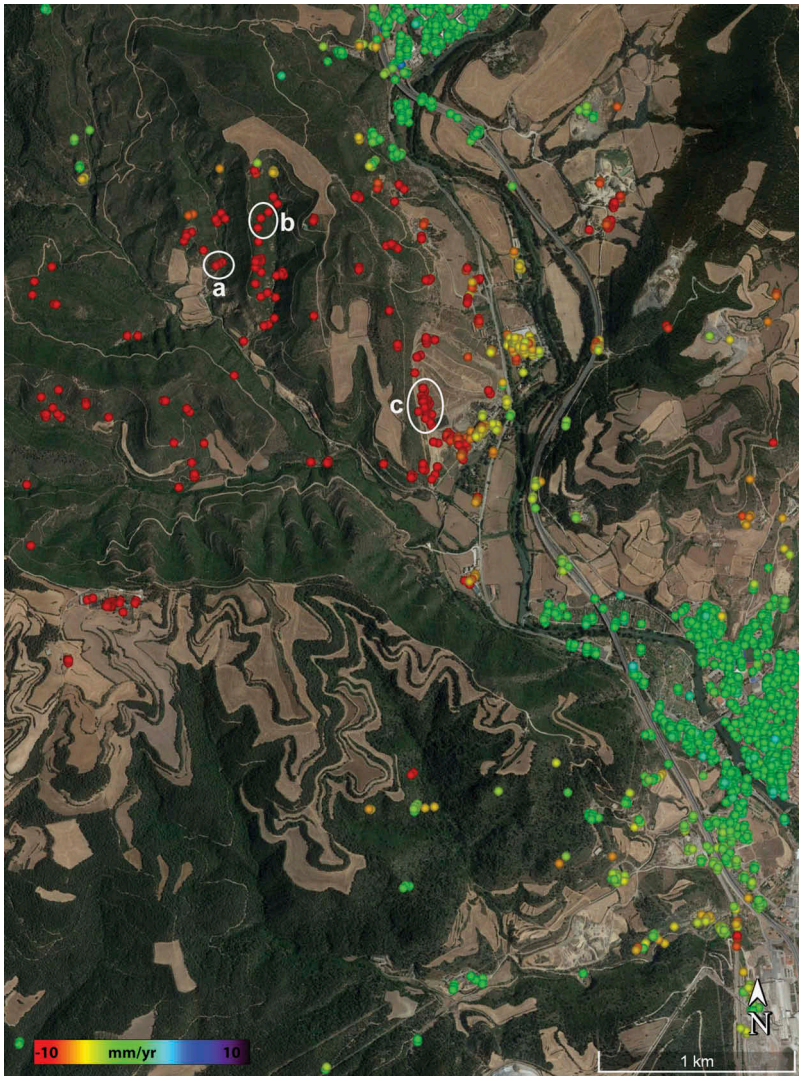

Figure 8. Color-coded and geocoded deformation velocity over the mining area of Sallent and Balsareny (Barcelona). The background image is an optical image from Google Earth. White circles show the position of the deformation time series of Figure 9.

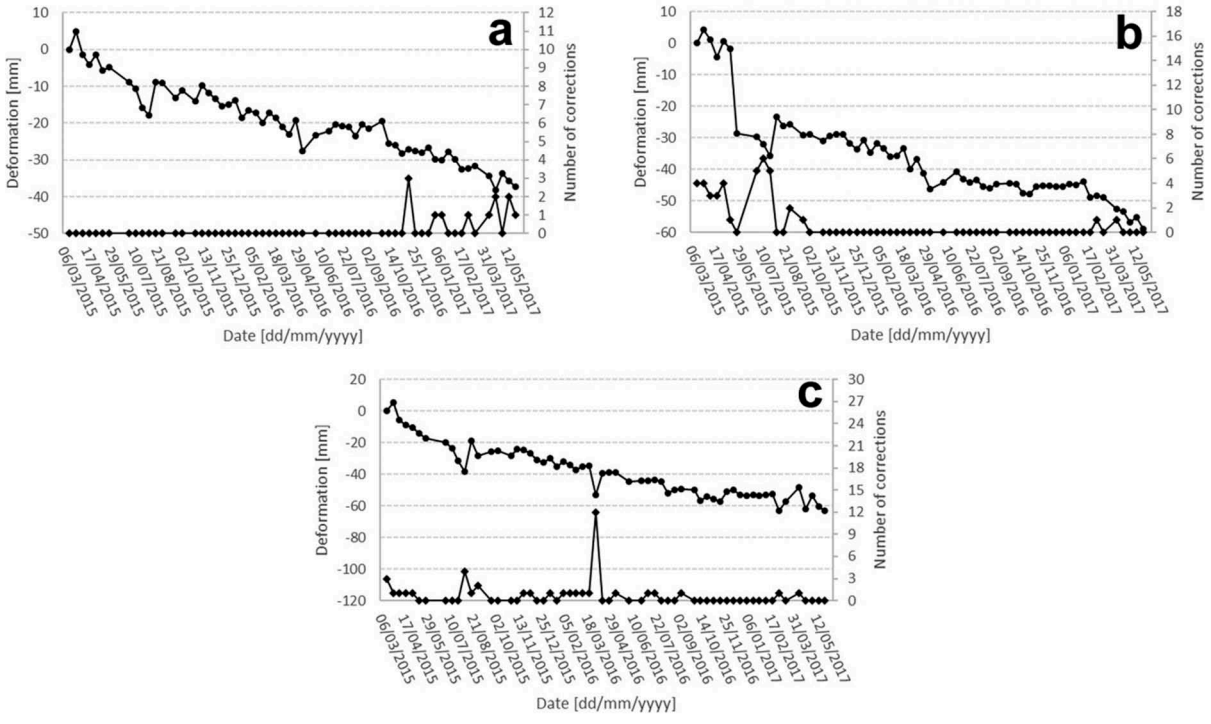

Figure 9. Three examples of time series of points located in the area shown in Figure 8 (see white circles). Each image of the time series (circles in the upper line) has associated a quality index (diamonds in the lower line).

intermediate PSI result (the stack of unwrapped image phases), can be used in the subsequent processing step (atmospheric filtering), to weight the relative importance of each processed pixel. This index can only be used with multi-look data.

- The generation of a quality index for each image of a given deformation time series. This provides a complete information that can be used to assess the quality and reliability of the time series. Several examples have been discussed in this paper. This quality index represents a valuable metadata, which can be used in the interpretation and exploitation of the PSI results.
- The generation of a quality index for the deformation time series. It concerns the overall quality of a final PSI product: the deformation time series. For this, it represents a useful metadata for the interpretation of the PSI results. It can be only generated using multi-look data.

Disclosure statement

No potential conflict of interest was reported by the authors.

Funding

This work has been partially funded by the European Union H2020 HEIMDALL Project, "Multi-Hazard Cooperative Management Tool for Data Exchange, Response Planning and Scenario Building" [Project N. 740689] and by AGAUR, Generalitat de Catalunya, through the Consolidated Research Group RSE, "Remote Sensing" (Ref: 2017-SGR-00729).

References

Baarda, W. (1968). *A testing procedure for use in geodetic networks. kanaalweg 4, rijkscommissie voor geodesie*. Delft: The Netherlands.

Barra, A., Monserrat, O., Mazzanti, P., Esposito, C., Crosetto, M., & Scarascia Mugnozza, G. (2016). First insights on the potential of Sentinel-1 for landslides detection. *Geomatics, Natural Hazards and Risk*, *7*(6), 1874–1883. doi:10.1080/19475705.2016.1171258

Barra, A., Solari, L., Béjar-Pizarro, M., Monserrat, O., Bianchini, S., Herrera, G., & Ligüerzana, S. (2017). A methodology to detect and update active deformation areas based on Sentinel-1 SAR Images. *Remote Sensing*, *9* (10), 1002. doi:10.3390/rs9101002

Bayer, B., Simoni, A., Schmidt, D., & Bertello, L. (2017). Using advanced InSAR techniques to monitor landslide deformations induced by tunneling in the Northern Apennines, Italy. *Engineering Geology*, *226*, 20–32. doi:10.1016/j.enggeo.2017.03.026

Berardino, P., Fornaro, G., Lanari, R., & Sansosti, E. (2002). A new algorithm for surface deformation monitoring based on small baseline differential SAR interferograms. *IEEE Transactions on Geoscience and Remote Sensing*, *40* (11), 2375–2383. doi:10.1109/TGRS.2002.803792

Björck, Å. (1996). *Numerical Methods for Least Square Problems*. Philadelphia, PA: Siam.

Costantini, M. (1998). A novel phase unwrapping method based on network programming. *IEEE Transactions on Geoscience and Remote Sensing*, *36*, 813–821. doi:10.1109/36.673674

Costantini, M., Farina, A., & Zirilli, F. (1999). A fast phase unwrapping algorithm for SAR interferometry. *IEEE Transactions on Geoscience and Remote Sensing*, *37*, 452–460. doi:10.1109/36.739085

Crosetto, M., Devanthéry, N., Cuevas-González, M., Monserrat, O., & Crippa, B. (2015). Exploitation of the full potential of PSI data for subsidence monitoring. *Proc. of Nisols, Ninth International Symposium on Land Subsidence*, 2015, November 15–19, Nagoya (Japan). Proc. IAHS, 372, 311–314, doi:10.5194/piahs-372-311-2015

Crosetto, M., Monserrat, O., Cuevas-González, M., Devanthéry, N., & Crippa, B. (2016). Persistent Scatterer Interferometry: A review. *ISPRS Journal of Photogrammetry and Remote Sensing*, *115*, 78–89. doi:10.1016/j.isprsjprs.2015.10.011

Dai, K., Li, Z., Tomás, R., Liu, G., Yu, B., Wang, X., & Stockamp, J. (2016). Monitoring activity at the Daguangbao mega-landslide (China) using Sentinel-1 TOPS time series interferometry. *Remote Sensing of Environment*, *186*, 501–513. doi:10.1016/j.rse.2016.09.009

De Luca, C., Bonano, M., Casu, F., Fusco, A., Lanari, R., Manunta, M., & Zinno, I. (2016). Automatic and Systematic Sentinel-1 SBAS-DInSAR Processing Chain for Deformation Time-series Generation. *Procedia Computer Science*, *100*, 1176–1180. doi:10.1016/j.procs.2016.09.275

Devanthéry, N., Crosetto, M., Monserrat, O., Cuevas-González, M., & Crippa, B. (2014). An approach to Persistent Scatterer Interferometry. *Remote Sensing*, *6*, 6662–6679. doi:10.3390/rs6076662

Ferretti, A., Prati, C., & Rocca, F. (2001). Permanent scatterers in SAR interferometry. *IEEE Transactions on Geoscience and Remote Sensing*, *39*(1), 8–20. doi:10.1109/36.898661

Förstner, W. (1986). Reliability, gross error detection and self-calibration. ISPRS commission III tutorial on statistical concepts for quality control. *ISPRS Int. Arch. Photogramm*, *26*, 1–34.

Gatelli, F., Monti Guamieri, A., Parizzi, F., Pasquali, P., Prati, C., & Rocca, F. (1994). The wavenumber shift in SAR interferometry. *IEEE Transactions on Geoscience and Remote Sensing*, *32*(4), 855–865. doi:10.1109/36.298013

Geudtner, D., Torres, R., Snoeij, P., Davidson, M., & Rommen, B. (2014). Sentinel-1 system capabilities and applications. In *Proceedings of IGARSS 2014*, Quebec City, Canada, 2014, July 13–18, 1457–1460.

González, P.J., Bagnardi, M., Hooper, A.J., Larsen, Y., Marinkovic, P., Samsonov, S.V., & Wright, T.J. (2015). The 2014–2015 eruption of Fogo volcano: geodetic modeling of sentinel-1 TOPS interferometry. *Geophysical Research Letters*, *42*(21), 9239–9246. doi:10.1002/2015GL066003

Huang, Q., Crosetto, M., Monserrat, O., & Crippa, B. (2017). Displacement monitoring and modelling of a high-speed railway bridge using C-band Sentinel-1 data. *ISPRS Journal of Photogrammetry and Remote Sensing*, *128*, 204–211. doi:10.1016/j.isprsjprs.2017.03.016

Monserrat, O., Crosetto, M., Cuevas, M., & Crippa, B. (2011). The thermal expansion component of Persistent

Scatterer Interferometry observations. *IEEE Geoscience and Remote Sensing Letters*, *8*, 864–868. doi:10.1109/LGRS.2011.2119463

Ng, A.H.M., Ge, L., Du, Z., Wang, S., & Ma, C. (2017). Satellite radar interferometry for monitoring subsidence induced by longwall mining activity using Radarsat-2, Sentinel-1 and ALOS-2 data. *International Journal of Applied Earth Observation and Geoinformation*, *61*, 92–103. doi:10.1016/j.jag.2017.05.009

Novellino, A., Cigna, F., Brahmi, M., Sowter, A., Bateson, L., & Marsh, S. (2017). Assessing the feasibility of a national InSAR ground deformation map of Great Britain with Sentinel-1. *Geosciences*, *7*(2), 19. doi:10.3390/geosciences7020019

Prats-Iraola, P., Scheiber, R., Marotti, L., Wollstadt, S., & Reigber, A. (2012). TOPS interferometry with TerraSAR-X. *IEEE Transactions on Geoscience and Remote Sensing*, *50*(8), 3179–3188. doi:10.1109/TGRS.2011.2178247

Scheiber, R., & Moreira, A. (2000). Coregistration of interferometric SAR images using spectral diversity. *IEEE Transactions on Geoscience and Remote Sensing*, *38*(5), 2179–2191. doi:10.1109/36.868876

Shirzaei, M., Bürgmann, R., & Fielding, E.J. (2017). Applicability of sentinel-1 terrain observation by progressive scans multitemporal interferometry for monitoring slow ground motions in the San Francisco Bay Area. *Geophysical Research Letters*, *44*(6), 2733–2742. doi:10.1002/2017GL072663

Torres, R., Snoeij, P., Geudtner, D., Bibby, D., Davidson, M., Attema, E., & Rostan, F. (2012). GMES Sentinel-1 mission. *Remote Sensing of Environment*, *120*, 9–24. doi:10.1016/j.rse.2011.05.028

Yague-Martinez, N., Prats-Iraola, P., Rodriguez Gonzalez, F., Brcic, R., Shau, R., Geudtner, D., & Bamler, R. (2016). Interferometric processing of sentinel-1 TOPS data. *IEEE Transactions on Geoscience and Remote Sensing*, *54*(4), 2220–2234. doi:10.1109/TGRS.2015.2497902